Orbital
The electronic journal of chemistry

the electronic journal of chemistry

Full Paper | http://dx.doi.org/10.17807/orbital.v16i3.20153

Green Synthesis of Polyesters Using Surfactant Catalysts in Microemulsions: The Role of Micelle Shape and Aggregation on Polymer Formation

Vadilson Malaquias dos Santos [a], Fabricio Uliana [a], Rayanne Penha Wandenkolken Lima [a], and Eloi Alves da Silva Filho* [a]

In this study, we explored traditional methods commonly found in the literature to analyze how surfactants and polymers interact during the synthesis of polyesters in emulsion systems. The study justifies its focus on micellar catalysis by exploring its effectiveness and suggesting methods for enhancing the synergy among surfactants, reactants, and catalys. We looked at factors like surface tension, critical micelle concentration, micelle shapes, aggregation numbers, and interfacial phenomena in the process of macromolecular packing in emulsion polycondensation. A surfactant-water system consisting of dodecylbenzenesulfonic acid and sodium dodecyl sulfate was employed. Polyesters were prepared from glycerol, ethylene glycol, diethylene glycol, and dicarboxylic acids in a surfactant-water system under mild conditions ranging from 70-150 °C. FTIR and 1H NMR confirmed the esterification. Differential scanning calorimetry indicated no crystallinity and a glass transition temperature range of −53 to −46 °C, typical of soft matter. The resulting polymers had molecular weights ranging from 1180 – 6800 g/mol. We found that these polymer aggregate shapes are able to respond by changing their sizes, both in bulk and at the air-solution interface, when the concentration of surfactant is increased above the critical micelle concentration. The results showed narrow spherical and ellipsoidal polymer aggregates, and the system was found to be suitable for green chemistry applications.

Graphical abstract

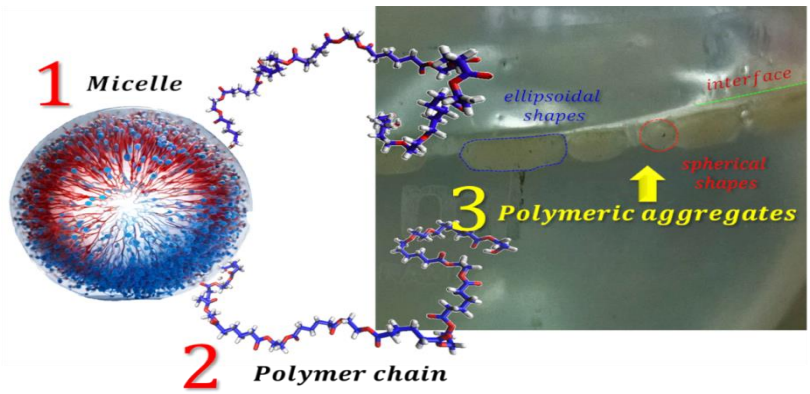

Keywords

Interfaces
Micellization
Polyesters
Surfactant

Article history

Received 31 Jan 2024
Revised 27 Aug 2024
Accepted 23 Sep 2024
Available online 08 Oct 2024

Handling Editor: Arlan Gonçalves

1. Introduction

Polyesters are considered to be one of the most adaptable polymers and have been widely used in sustainable and eco-

[a] Department of Chemistry, Federal University of Espírito Santo (UFES), Av. Fernando Ferrari, 514 Goiabeiras, 29075-910, Vitoria, Brazil.
*Corresponding author. E-mail: **eloisilv@gmail.com**

friendly materials. Polyesterifications are reactions between dibasic acids and diols or their derivatives, as well as alcoholysis and acidolysis of low-molecular-weight esters, alcoholysis of acyl chlorides, ring-opening polymerization, enzymatic polymerization, and elevated temperatures above 150 °C with alcohol or water being efficiently and continuously removed, while organic catalysts or conventional metal catalysts are usually applied. Direct polyesterifications generally require catalysts such as antimony, germanium, titanium, and aluminum compounds, as well as organometallic compounds of tin, lead, and titanium, such as titanium butoxide, titanium isopropoxide, and dibutyltin oxide. However, a more flexible and convenient path exists for the environmentally friendly production of polyester. This involves obtaining polyesters through an in-water/micelle system in the presence of a surfactant catalyst under mild conditions below 150 °C. This method is especially useful for greener synthesis than the previously mentioned methods [1-7]. A microemulsion can be created by either significantly increasing the concentration of surfactant in the system or significantly decreasing the concentration of water-insoluble monomer. Microemulsions of monomers are stable systems in which all of the monomers are contained within the micelles. At extremely high concentrations of surfactant, the surfactant may create a continuous network rather than distinct micelles [8].

Surfactants are amphiphilic molecules that can spontaneously self-assemble in solutions of water or organic solvent, forming aggregates called micelles. This phenomenon occurs due to the thermodynamic stability of the system and the decay of its free energy when compared to its unassembled components. However, the self-assembled structure is not necessarily the equilibrium structure [9-12]. According to Larsson *et al.* (2021) [10], the surfactant configuration affects the morphology of the micelle, and entanglement of worm-like micelles often leads to strong modifications of the rheological behavior of the system. The precise arrangement of micelles will depend on the structures of the molecules involved, temperature, pH, electrolyte type and concentration, shape of the surfactant, and other factors that affect the geometries of aggregates in the micelles. The aggregates that spontaneously self-assemble form a large type of aggregate such as spherical, sphero-cylindrical, ellipsoidal, wormlike, lamellae or 3D entangled network structures, resulting in the different viscoelastic behavior of these solutions. [8-13].

The interactions between newly synthesized polymers and surfactants in aqueous media give rise to the formation of association structures, thereby modifying the solution, micelles shapes, and interfacial properties. These changes are caused by the hydrophobic attraction between the surfactant tails and polymer segments, leading to a decrease in free energy at the hydrocarbon-water interface, partial protonation of oxygen atoms in the polymer chain, and electrostatic attraction between the polymer segments and surfactant head groups [13-15]. The association between polymers and micelles is disfavored by steric and electrostatic repulsions at the interface, as well as the overlapping effects of their hydration shells. The degree of association is determined by the interplay and competition among these forces [13, 16].

The structure of a linear polymer chain can be characterized using different molecular descriptors, including those that detail its size and shape [17]. The polymer has a diverse range of conformations available to it and can exhibit varying degrees of flexibility as a result of its capacity for bending and twisting in different directions. End-to-end descriptors are defined as the vector sum of all molecular bond vectors. For bond vectors $\vec{b}_i = r_{i+1} - r_i$ between the center of the monomer (i) and $(i+1)$, where (N) is the number of bond chains and $(n = N-1)$, we have:

$$R_{ee} = \sum_{i=1}^{n} \vec{b}_i \qquad (1)$$

The radius of gyration is a well-defined size descriptor for complex polymeric structures [17] (branched or ring-shaped), where all monomers have defined masses, with the radius of the center of mass given by (r_{CM}).

$$\mathbf{R_g^2} = \frac{\mathbf{1}}{\mathbf{N}} \sum_{\mathbf{i=1}}^{\mathbf{N}} (\mathbf{r_i} - \mathbf{r_{CM}})^2 \qquad (2)$$

Although there have been many studies conducted, it has been challenging to provide a clear microscopic explanation of the catalysis mechanism of polymerization in micelles and the polymer aggregation phenomenon in spherical and ellipsoidal aggregates. This is because most experimental investigations have focused on measuring macroscopic phase behavior, such as changes in viscosity and conductivity resulting from a decrease in the critical micelle concentration (CMC). The interaction between the polymer and surfactant is determined by observing the critical aggregation concentration (CAC), which is typically lower than the CMC of pure surfactant solutions.

In the present work, polyesters were prepared from adipic acid (AD), glycerol (GLY), and ethylene glycol (EG) in a surfactant system of DBSA and SDS in microemulsions of water/surfactants. We found a correlation between changes in the polymeric aggregate's sizes and shapes, the surface tension behavior, micelle shape, and surfactant concentration. The experimental results of polyester synthesis revealed polymer aggregates that were relatively narrow spherical and ellipsoidal: prolate ellipsoidal $(\mathrm{R}_a > \mathrm{R}_b = \mathrm{R}_c)$ and tri-axial ellipsoidal $(\mathrm{R}_a \neq \mathrm{R}_b \neq \mathrm{R}_c)$. The MD technique is used in this paper to investigate the interaction of an anionic SDS and DBSA micelle with a polymer, Poly(ethylene adipate) and PEG, an aliphatic polyester synthesized from a polycondensation reaction between ethylene glycol and adipic acid. Density Functional Theory (DFT) method was used to characterize the electronic structure of the SDS and DBSA. The aim of this study is to show that the synthesis of polyesters through the use of surfactant catalyst systems is strongly influenced by micelle shapes, aggregation numbers, and H-bonds.

2. Results and Discussion

2.1 Polymers characterization

Instrumental analysis of polymers and composites was carried out using Fourier Transform Infrared spectroscopy (FTIR), ^{1}H NMR, differential scanning calorimetry (DSC), density and viscosity measurements. The ^{1}H NMR proton signals of 2.60 ppm and 3.65 ppm is typical of polyesters. The ^{1}H NMR spectra display the anticipated signals between 1.4 – 2.2 ppm, which correspond to the aliphatic chains of adipic acid in poly(glycerol adipate) (PGA) and poly(ethylene adipate) (PEA). Additionally, signals indicating deshielded CH_2 and CH protons from di- and triacyl glycerol are observed in the 3.0 – 4.5 and 4.5 – 5.5 ppm regions, respectively. To investigate the differences in the chemical structure of the

synthesized polyesters, FTIR spectroscopy was implemented. The polymers synthesized from the reaction between ethylene glycol (EG) and adipic acid (AD) formed as PEA, an aliphatic polyester, with densities between $(1.183 - 1.216)\mathrm{g/mL}$ at 25 °C, a glass transition temperature (T_g) between $-46/-50$ °C, a crystalline melting temperature (T_c) between $30/38$ °C, and a molecular weight between $1367 - 1991\ \mathrm{g/mol}$. The reaction between AD and DEG produces poly(diethylene glycol adipate) (PDEG), which has a T_g of $-51/-53$ °C and a molecular weight of $2577 - 2751\ \mathrm{g/mol}$. The PGA, synthesized from reactions with GLY/AD have molecular weights between $2500 - 3200\ \mathrm{g/mol}$.

The synthesized PEG obtained a molecular weight of $5{,}100 - 6{,}800\ \mathrm{g/mol}$, equivalent to the commercial polyethylene glycol PEG6000 and $6{,}350 - 7{,}567$ g/mol for copolymers (citric acid)-PEG. The polyesters molecular weights and intrinsic viscosity were determined for Mark-Houwink-Sakurada (MHS) relation [18]. Polymer molecular weight reflects the number of entanglements of polymer chains in solution, thus solution viscosity. The polymers synthesized in the aqueous/surfactant phase had a T_g between $-53/-50$ ℃, which indicates their instability and softness. Amorphous polymers tend to behave in an elastic manner at low temperature in the glassy state. The mechanical properties of these GLY, EG or DEG and diacids polycondensation products are highly dependent on the diacid monomers employed, the synthesis parameters, as well as of the curing conditions employed, however, the synthesized samples have soft matter characteristics, low hardness and elasticity like shows that Figure 1. Figure 1(A) shows a hydrogel prepared with PEG/AC/ionic liquid prepolymer, with high viscosity at 25 ℃. In Figure 1(B) we have a solid material prepared from PEG/AD. This Figure 1 shows the versatility of the synthesized materials.

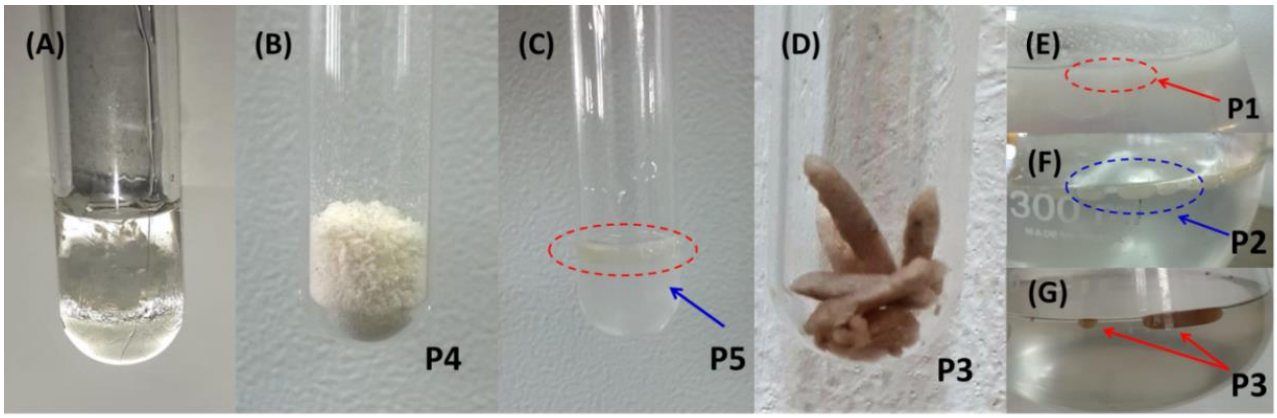

Fig.1. Shows the different shapes of polyesters after synthesis. (A) PEG/AC/ionic liquid prepolymer, hidrogel (B) PEG/AD, catalysts DBSA/H_2SO_4 (C) Prepolymer PEA, polyester P5 (D) shape prolate ellipsoidal of polyester by the reaction of GLY+AD, catalysts SDS/H_2SO_4, (E) Solid particulate material on the surface of the water/SDS reaction medium, after 20h of mechanical stirring at 85 °C - using $SnCl_2$ as cocatalyst, polyester P1 (F) Semi-solid vesicles with an ellipsoid appearance formed after 20h of mechanical agitation at 75℃, water/SDS reaction medium using sulfuric acid as H_2SO_4 cocatalyst, polymer P2 (G) shape oblate spheroids and ellipsoids of polyesters in gel point, polymer P3.

Esters have a pattern of three intense peaks at 1700 cm^{-1}, 1200 cm^{-1}, and 1100 cm^{-1} from the C=O and two C–O stretches. Esters and aldehydes are frequently encountered examples of molecules that exhibit a C=O stretching frequency (1735cm^{-1}, 1725cm^{-1} and 1715 cm^{-1} respectively) are too close to allow a clear distinction between them. However, aldehydes can be distinguished by examining both the presence of the C-H of an aldehyde (2750 and 2850 cm^{-1}) and the presence of a carbonyl group. The absorption due to the $-CH_2$ and CH groups of the un-reacted and esterified GLY are seen in envelop at ranges $2950 - 2875\ \mathrm{cm^{-1}}$, stretch C–H, sp^3. For polyester P1 and P2, the absorption in the range of $1734 - 1176\ \mathrm{cm^{-1}}$ is related to C=O and C–O of ester groups [10, 11].

The Figure 2 shows the typical FTIR spectra for AD and synthesized PEA samples, where all exhibit peaks in the region of $3357\ \mathrm{cm^{-1}}$, (associated with OH deformation), between $1175 - 1715\ \mathrm{cm^{-1}}$, (axial deformation vibrations of double bonds), and at $2852 - 2915\ \mathrm{cm^{-1}}$, (associated with ester groups, $C - O - O - C$ bonds, and CH, bonds, respectively). The FTIR for sample PEA-3 differs from the other two samples, with peaks at, $2852 - 2915\ \mathrm{cm^{-1}}$ (axial deformation vibrations of hydrogen atoms in the $C - H$ groups), $1635\ \mathrm{cm^{-1}}$ (vibration of the $C = O$ group), and $906 - 966\ \mathrm{cm^{-1}}$ (axial and angular deformations of $C - O$ bonds). The main absorptions observed in the spectrum of the PEG and their attributions are: 2980–2950 cm^{-1} – CH_2 and $-CH_3$ vibration stretch; 1736 – 1726 cm^{-1} C = O stretch; 1480 – 1400 C – C vibration stretch; 1200 – 1100 cm^{-1} C – O, sp^3, alcohol bond; 1087 –1036 cm^{-1} C – H in plane and 876 – 815 cm^{-1} C – H deformation vibration.

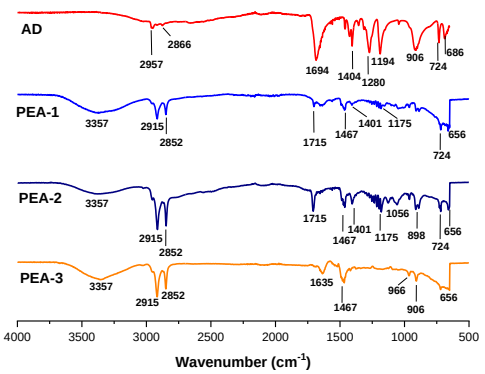

Fig.2. FTIR spectra of Adipic Acid (AD) and Polyester (PEA 1-3). The main peaks associated with the structures are highlighted. SDS concentration: 10%, 20% and 40% above the CMC, respectively.

2.2 Thermodynamic aspects of reactants, surfactants, micelles and polymers interactions

The typical reaction medium used in this study is composed of diols, triols, and dicarboxylic acids. In this context, there are several studies on the thermodynamic properties of the reactants or even some polymers, such as PEG in micellar systems [19-25]. The formation of the polymer chain and the presence of surfactants affect the surface tension and interfere with the formation of the polymer aggregate. Figure 3 illustrates the plot of experimental surface tension values (γ) against the logarithm of the concentration of surfactant ([SDS]; mol/L) for SDS-water, 30% EG-H_2O and PEG-H_2O. The observed pattern is a typical indication of solutions that form micelles in SDS-water system, which can be accurately described by the expression, with $g(C)$ is 1for $C \leq CMC$ or 0 $C \geq CMC$ [19]:

$$\boldsymbol{\gamma(C) = -A[\ln(CMC) - \ln(C)]g(C) + \gamma_0} \qquad (3)$$

In concentrations of surfactant above the CMC, γ_0 denotes the surface tension. The change in surface tension in relation to the natural logarithm of the surfactant concentration, C, is expressed as $A = \partial\gamma/\partial \ln C$, which is the slope value.

The excess surface concentration described by the Eq. 4, where T is the temperature, R is the gas constant and k =2 for ionic surfactant [19]:

$$\boldsymbol{\Gamma = \frac{-A}{kRT}} \qquad (4)$$

$$\boldsymbol{A_{min} = \frac{1}{\Gamma N_A}} \qquad (5)$$

The Eq.5, $\mathbf{A_{min}}$ is minimum area per molecule at the air/water interface, where $\mathbf{N_A}$ is the Avogadro number. The SDS-water data in Figure 3 is fitted to the function (3) with the varied, $\mathbf{CMC = 8.01 \times 10^{-3}\ mol/L}$; $\mathbf{A = 4.78\ mN/m}$ and $\boldsymbol{\gamma_0} = \mathbf{22.90\ mN/m}$. The excess surface for SDS is $\mathbf{9.65 \times 10^{-6}\ mol \cdot m^{-1}}$ and $\mathbf{A_{min}}$ is $\mathbf{1.72\ nm^2}$. For the SDS–polymer system,$\mathbf{CAC = 4.95 mmol/L}$; $\mathbf{A_{min} = 9.62\ mN/m}$ and $\boldsymbol{\gamma_0} = \mathbf{34.03\ mN/m}$.

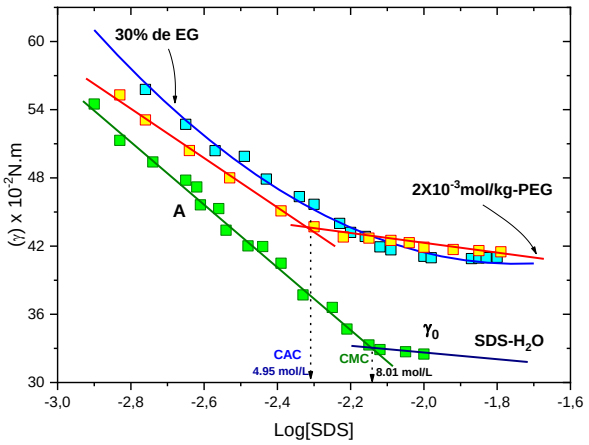

Fig.3. Surface tension as a function of concentration for SDS in water, 30% EG-H_2O and 2 $\times 10^{-3}$ mol/kg polyethylene glycol PEG6000 at 25 °C.

The excess surface for SDS–polymer is $\mathbf{1.94 \times 10^{-6}\ mol/m}$ and $\mathbf{A_{min} = 85.4\ nm^2}$. For DBSA, $\mathbf{CMC = 5.49 \times 10^{-4}\ mol/L}$, $\mathbf{A = 6.60\ mN/m}$ and $\boldsymbol{\gamma_0} = \mathbf{33.0\ mN/m}$. The excess surface for DBSA system is $\mathbf{1.32 \times 10^{-6}\ mol \cdot m^{-1}}$and $\mathbf{A_{min} = 1.23\ nm^2}$. According to [20], micelle structural parameters of DBSA-PEG, for sample 5 vol% of PEG, CAC is approximately$\mathbf{2.0 \times 10^{-4}\ mol/L}$; $\mathbf{N_{agg} = 64}$; $\boldsymbol{\gamma} = \mathbf{1.5}$; $\boldsymbol{\alpha} = \mathbf{0.19}$; $\mathbf{k_d = 0.40\ nm^{-1}}$ and polymer/micelle ratio $\boldsymbol{\delta} = \mathbf{0.6}$, for $\boldsymbol{\delta} = \mathbf{N_{PEG}/N_{mic}}$, where $\mathbf{N_{PEG}}$ and $\mathbf{N_{mic}}$ are the number densities of PEG and micelle fractions.

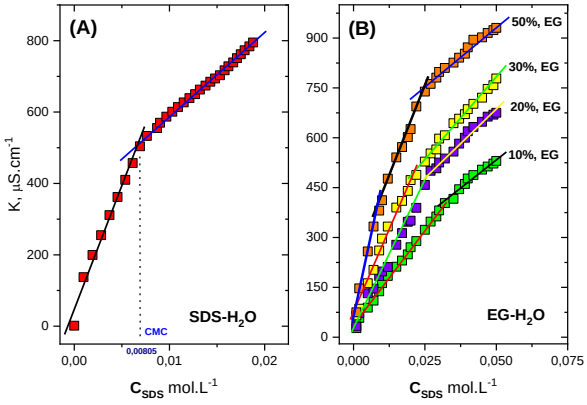

Fig.4. Specific conductivity vs C_{SDS}, at 25 °C, plots for (A) SDS-H_2O (B) SDS, EG-H_2O reaction system.

The Figure 4 shows the conductivity profiles for SDS in the absence of aqueous mixtures of ethylene glycol (EG) or in the presence of 10%, 20%, 30%, and 50% EG. The specific conductivity increases sharply in the pre-micellar region with surfactant concentration but is somewhat reduced at certain concentrations, which reflects the CMC for SDS aqueous solution. Table 1 shows activation energy of the EG-H_2O system. The relationship between conductance (σ), activation energy (E_a), and temperature (T) was calculated using an Arrhenius-type equation, $\sigma = \sigma_0 \exp -(E_a/RT)$, where σ_0 is constant for a surfactant [21].

Table 1. Activation energy of the SDS-EG-H_2O reaction system.

EG (wt%)	$E_a(CMC_i)$ (kJ. mol^{-1})		$E_a(CMC_f)$(kJ. mol^{-1})	
	Exp.	Ref.[33]	Exp.	Ref. [21]
0	10.1	9.0	24.1	23.4
10	13.2	12.9	20.5	20.2
20	19.9	19.2	23.9	26.6
30	18.9	18.7	26.4	23.6
50	26.5	–	23.5	–

The enthalpy and entropy of micellization (ΔH^0_{mic} andΔS^0_{mic}) were calculated from the following equations: (6) and (7), and the Gibbs free energy of the effect of a cosolvent EG on the micellization process from (8) [21].

$$\Delta H^0_{mic} = (2-\alpha)R\left[\frac{\partial \ln x_{CMC}}{\partial(1/T)}\right] \qquad (6)$$

$$\Delta S^0_{mic} = \frac{(\Delta H^0_{mic} - \Delta G^0_{mic})}{T} \qquad (7)$$

$$\Delta G^0_R = \Delta G^0_{mic(Mix)} - \Delta G^0_{mic(água)} \qquad (8)$$

According to Gracie *et al.* [21], the reason for the increase in E_a following the CMC is attributed to several factors, such as the binding of counterions with the micelle, the effective level of dissociation of the counterion (β), the micelle's radius and the viscosity of the solvent system. When EG concentrations are elevated, the effective degree of micellar

dissociation (β) rises, resulting in a greater number of free Na^+ ions to conduct the current. Additionally, the aggregation numbers decrease as EG content increases, which allows for a lower value of E_a. The micellization process appears to be less favorable in EG and water mixtures, as indicated by the positive values of ΔG_R^0, (Table 2).

Table 2. Thermodynamics of SDS micellization in the EG-H_2O system

EG (wt%)	CMC ($\times 10^{-3}$ mol/L)		ΔG_{mic}^0		ΔG_R^0		ΔH_{mic}^0		ΔS_{mic}^0	
	Exp.	*Ref.*	*Exp.*	*Ref.*	*Exp.*	*Ref.*	*Exp.*	*Ref.*	*Exp.*	*Ref.*
10	8.0	8.2	−33.9	−33.3	2.80	3.35	−11.0	−11.5	73.5	73.1
30	10.1	10.7	−28.1	−28.3	8.60	8.35	−12.9	−13.0	51.0	53.4
50	17.9	18.7	−23.5	−23.7	13.20	12.95	−14.0	−13.9	31.8	32.9

The energy values are in $kJ.mol^{-1}$, with the exception of entropy which is at $J.K^{-1}.mol^{-1}$. Ref. [21]

The parameters of micellization are determined based on the degree of ionization in the micelle (α), which is determined by the Evans' ratio ($\alpha = S_2/S_1$) - the ratio between the slopes of the micellar and pre-micellar phases, where S_2 and S_1, are the slopes of micellar and pre-micellar phases, respectively [22], and the degree of counter ion binding, $\beta = (1 - \alpha)$. In the cases under study, the surfactant functions as a catalyst for the reaction. Micellization parameters for SDS, aggregation numbers (N_{agg}) and the micellization constant (K_C) are described in the literature [22]. As the temperature rises, the enthalpy of micellization transitions from being endothermic to being exothermic. This phenomenon has been previously noted in both cationic and anionic surfactant micellization. The alteration in the enthalpy sign with temperature is a characteristic of hydrophobic bonding. On the other hand, the Gibbs energy of micellization, which is connected to the critical micelle concentration through $\Delta G^0 = RT\ln(CMC)$, is much less sensitive to changes in temperature. This can be attributed to enthalpy/entropy compensation that arises when there are numerous molecular configurations with comparable free energy.

If the surfactant concentrations are high, the surface tension behavior changes due to precipitation and additional complexation. The excess of surfactant makes it possible to recover a single solution, and the surface tension is dominated by the high concentration of surfactant. Nevertheless, precipitation, particularly involving polyelectrolytes, could negatively affect equilibration in these systems. Summing up, the formation of colloids during the precipitation step can result in a metastable suspension instead of redissolution [25, 26]. The addition of ionic liquid significantly influences the surface-activity and aggregation behavior of surfactants. According to Peacock *et al.* [26] in the case of oppositely charged polymers and surfactants, the electrostatic contribution may result in a sufficiently high driving force for monomer binding, e.g., It could be expected that the dodecyl sulfate ions will bind to the protonated charged groups of the polymers, but it could be PEG-SDS will bind with an H-bond. The driving force of hydrogen-bonding interactions exists in diverse assembly systems, and micelles serve as the H-bond acceptor when assembled under acidic conditions [27]. The hydrophobic effect could significantly increase the apparent reaction rates and improve selectivity when conducting reactions within micelles [28, 29]. According to Tang *et al.* [28], thermodynamic and kinetic analyses indicated that rate increases in micellar reaction media occurs with the participation of the surfactant as an acid-base catalyst, as well as changes in the structures of the transition state in the micelle compared to the reaction performed in a solvent.

2.3 MD simulation

This section utilizes the MD simulation findings to examine various elements such as the structural parameters, the micellization process of SDS and DBSA, the impact of solvation on reactants, and the dynamics between the polymer and surfactant. Figure 5 shows the micelle systems and snapshots obtained at 20 and 70 ns of the MD trajectory. For this simulation study, the aggregation number is set at 64 – 67 for SDS and 80 – 98 for DBSA, Figure 5 (A) and (C), respectively, as has been found in experiments [16, 20,24,30-33].

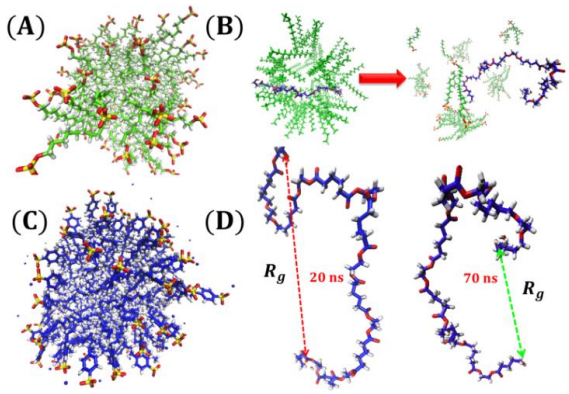

Fig.5. MD results (A) Snapshot obtained at 70 ns of the MD simulation for SDS micelles, $N_{agg} = 67$ (B) Snapshot obtained at 20 and 70 ns for interaction SDS-Oligomer PEA (C) Snapshot obtained at 70 ns for DBSA spherical micellar aggregate, $N_{agg} = 80$ (D) Radius of gyration for snapshot interaction of SDS-Oligomer PEA at 20 and 70 ns.

The oligomers of PEA, Figure 5(B), were manually inserted into the center of the micelle to generate the initial conformations not shown in (0 ns). Figure 5(B) shows a snapshot obtained at 20 and 70 ns for the interaction SDS-oligomer PEA. Comparing the initial and final micellar conformations, we note that the relative position between the host and guest molecules was totally changed after the simulation time. Moreover, it could be seen that micelle rupture occurred at a very fast timescale, i.e., approximately 10 ns. We anticipated these results because the inner cavity of SDS is hydrophobic and the radius of PEA is larger than that of the micelle. Micellar aggregation is highly flexible and can exhibit a broad range of bending angles because of the strong electrostatic coupling. This Figure 5 (D) shows the final snapshot separated from the micelle obtained from the MD trajectory of 50 ns of PEA-oligomer. The R_g decreased from 4.46 nm to 3.43 nm. The chain conformation of PEA is

affected by an aqueous solvent, so in the TIP3P or SPC water model. Poly(ethylene adipate) is insoluble in water, polymer-polymer self-interactions are preferred, and the polymer coils will contract. For the polymers, the experimental solubility parameter is treated as a vector composed of three components: dispersion (δ_d), polar bonding (δ_p), and hydrogen bonding (δ_h). The end point of the radius vector thus represents Hildebrand's solubility parameter (δ_0) in the three-component space [34].

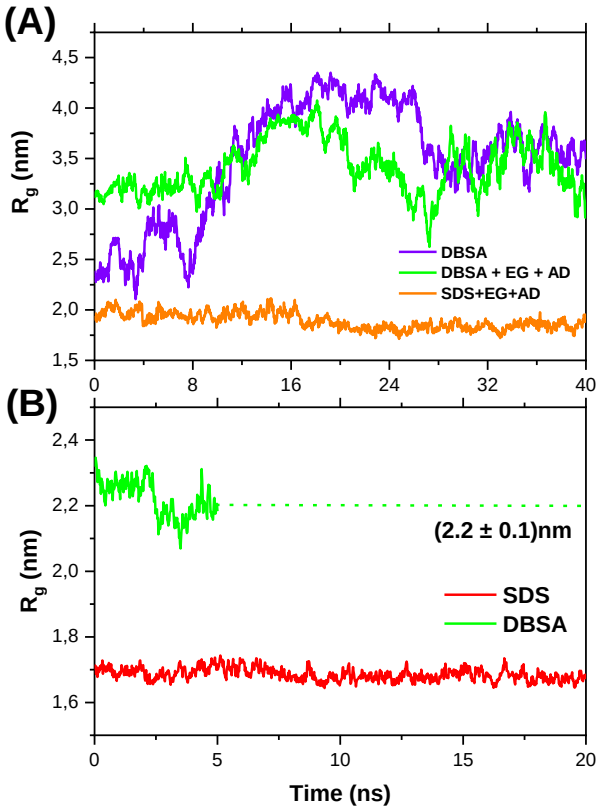

Fig.6. MD Trajectory of the average radius of gyration of SDS and DBSA systems (A) Temperature range [298 - 343] K (B) At 298 K.

Figure 6 shows a MD Trajectory of the average radius of gyration of SDS and DBSA systems. The simulation allows us to calculate the average size of micelles by considering the aggregation number and the radius of gyration of both the SDS and DBSA systems at each step. Considering each moment of the MD trajectory, there is a clear indication that a small structural rearrangement occurred in the first 40 ns of the simulation for the DBSA/EG/AD system.

In the Figure 7, there is a correlation between the number of H-bonds formed in the heads of the micelles and the hydrogen bonding relationships for the reactants. In Figure 8 we plot the accessible surface area (SASA) of micelles and reactants. At temperature range (298 - 343) K, the average SASA´s of SDS, reaction system 1 (SDS + reactants) and DBSA micelles were $SASA_{SDS}^{range}$: $(104-120)\ nm^2$; $SASA_{DBSA}^{range}$: $(163-166)\ nm^2$and $SASA_{1}^{range}$: $(120-129)\ nm^2$. At 293K, the average SASA's of SDS, reaction system 2 (DBSA + reactants) and DBSA micelles were $SASA_{SDS}^{total} = 104\ nm^2$; $SASA_{DBSA}^{total} = 163\ nm^2$ and $SASA_{2}^{total} = 132\ nm^2$, as depicted in Fig. 8. Hydrophobic interactions, the infiltration of water or other polar species, and H-bonds are involved, and they are assumed to be the fundamental driving force of many chemical and biological phenomena in micelle environments.

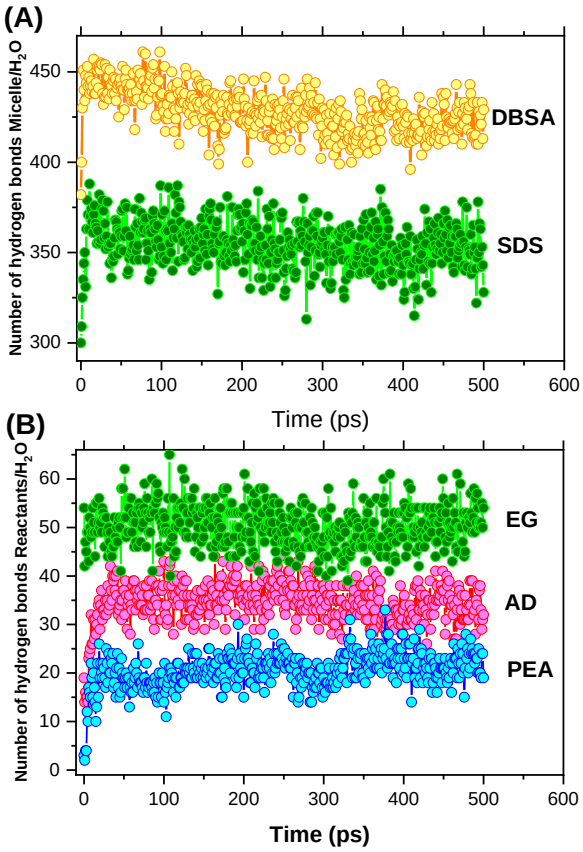

Fig.7. The number of hydrogen bonds between micelles and reactants molecules as a function of time. (A) SDS and DBSA micelles (B) EG, ethylene glycol; AD, adipic acid, and PEA, poly(ethylene adipate).

The shape of micelles is analyzed using the radius of gyration, which is calculated using the relation (2). Assuming spherical micelles with constant density, there is a linear relationship between micelle radius R_{mic} and the radius of gyration, equation (9), where r_i is the position of a particle in a micelle consisting of N particles and r_{CM} is the center-of-mass for the micelle. The geometric radius of a micelle (R_{mic}) is calculated from equation (9) [12]. The shape and stability of micelles are related to their eccentricity, ε, which is defined as (10), were I_{min} is the moment of inertia along the principal axes with the smallest magnitude, I_{avg} is the average of all three moments of inertia. When $\varepsilon = 0$ or $I_{max}/I_{min} = 1$, the micelle has a perfectly spherical shape. Conversely, if $\varepsilon = 1$, the micelle has an ellipsoidal shape [35,36]:

$$R_{mic} = \sqrt{\frac{5}{3}}\langle R_g \rangle \qquad (9)$$

$$\varepsilon = 1 - \frac{I_{max}}{I_{min}} \qquad (10)$$

The eccentricity parameters are (0.12 ± 0.05) for SDS, micelles of size $N_{agg} = 67$ and (0.13 ± 0.03) for DBSA, $N_{agg} = 80$. As the aggregation number of SDS micelles increases to a value ≥ 92, the micelles transform into a more ellipsoidal shape [36]. This transformation is apparent from the rise in the eccentricity factor. The ε values obtained in this work are similar to those values found in literature [36, 37].

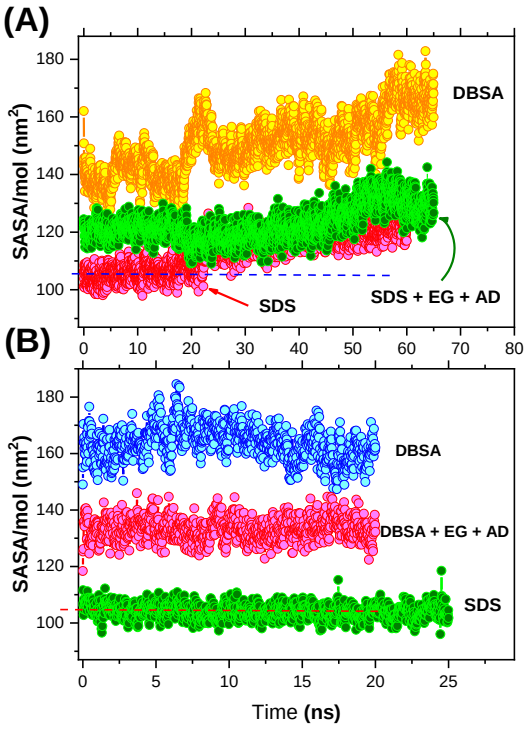

Fig.8. Accessible surface area for (A) SDS and DBSA micelles, and reaction system: SDS micelle + reagents. Temperature range [298 - 343] K (B) SDS and DBSA micelles, and reaction system: DBSA micelle + reagents. At 298 K.

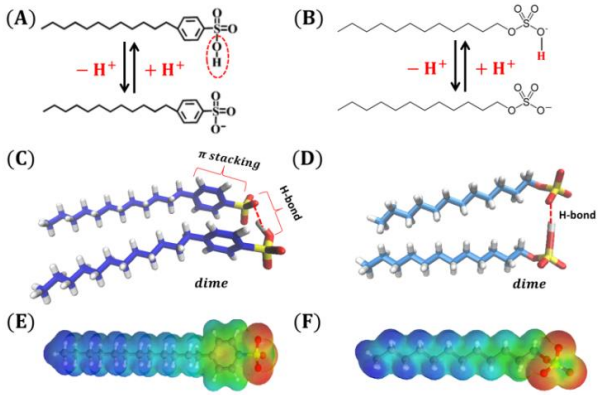

Fig. 9. The surfactant structure of the main used components studied in this work **(A) (B)** Acid–base equilibrium of dimers DBSA and SDS **(C) (D)** π stacking and H-bond of DBSA-dimer and H-bond of SDS- dimer **(E) (F)** Molecular Electrostatic Potential (MEP) is calculated at the DFT B3LYP/6-311G+(2d,p) level of theory for DBSA and SDS.

The interaction of water molecules with the micelle is dominated by interactions with the hydrophilic head group. Figure 9 shows acid–base equilibrium of dimers DBSA and SDS. The molecular electrostatic surface map (MEP) results are depicted in Figure 9 (E-F). The molecular electrostatic surface map is associated with the total electron density, and used in predicting regions of nucleophilic and electrophilic attack as well as H-bonding interactions. The order of potential increase is from red < orange < yellow < green < blue. Areas of negative charge, indicated by red and yellow colors, show electrophilic reactivity, while areas of positive blue charge in MEP show nucleophilic reactivity.

There exists a zone at the boundary of the micelle interior and the bulk water where the water molecules interact with both the hydrophilic head group and the hydrophobic tail of the micelle. This region is of great interest when comparing SDS and DBSA micelles, since there are not enough head groups to cover the entire surface of the micelle. In DBSA micelles, the region is occupied by aromatic rings that serve as a buffer, leaving the hydrophobic tail region devoid of water molecules. The formation of H-π interactions drives this interaction, which cannot occur with the aliphatic surfactant component [37, 38]. This absorbing region may play a significant role in the performance of DBSA micelles in contrast to SDS ones, particularly when used as catalysts for polymer synthesis, as well as in the infiltration of molecules inside the micelle when used as microreactors [37].

The root mean square deviation (RMSD) measures how the micelle system deviates from initial reference geometry, as depicted in Figure 10. Both time series show the RMSD levels off at approximately 1.29 nm for DBSA micelles and DBSA-PEA systems, indicating that the structure is relatively stable and SDA-PEA is instable for a range of 45–65 ns (Figure 10 A). DBSA-reactants and DBSA-micelles, levels off at 0.81 nm and 0.22 nm for the SDS-PEA system—SDS micelle, indicating very stable conformations (Figure 10 B).

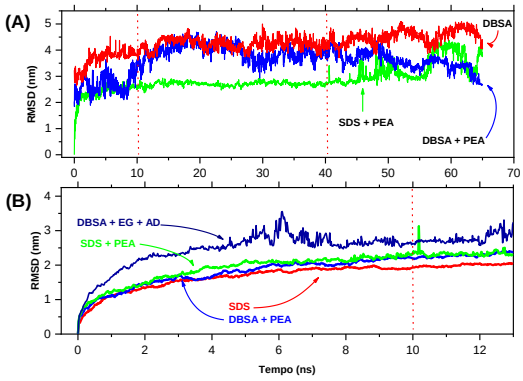

Fig. 10. Chemical (A) Temperature range [298 - 343] K (B) Constant temperature [298] K

2.3 Electronic structure of reactants

The electronic structure of the surfactants and reactants was investigated by DFT calculations (Table 3). The HOMO (highest occupied molecular orbital) and LUMO (lowest unoccupied molecular orbital) energies are of very important significance in delineating quantum characteristics like ionization potential ($IP = -E_{HOMO}$), electronic affinity ($EA = -E_{LUMO}$), electronegativity, electrophilicity, and several others. As per Koopmans' theorem [39], the IP can be derived from the absolute value of the HOMO energy, while the EA is roughly equivalent to the negative of the LUMO energy. A lower IP value in the case of surfactants indicates their superior capacity as electron donors.

The stability of the compounds can be evaluated through their energy gap ($E_g = |\varepsilon_{HOMO} - \varepsilon_{LUMO}|$), with a higher E_g indicating higher stability and a lower E_g indicating higher reactivity. Comparatively, DBSA is a more effective catalyst than SDS. The $HOMO - 1$ and $LUMO + 1$ orbitals are energetically important in the micelle formation process. SDS has a greater capacity for stacking at the liquid interface because it is more stable. On the other hand, the EG and DEG reagents have similar E_g values, but the EG molecule has several conformations in a liquid medium (α, β, and γ) [40], which must be taken into consideration in a reaction

mechanism. Density functional theory (DFT) is employed to calculate the global reactivity descriptor, providing insights into the overall behavior of molecules. These quantum molecular descriptors include, electronegativity ($\chi = -(E_{LUMO} + E_{HOMO})/2$), electronic chemical potential ($\mu = -(E_{LUMO} + E_{HOMO})/2$), global hardness ($\eta = -(E_{LUMO} + E_{HOMO})/2$), softness chemistry ($s = 1/2\eta$), electrophilicity ($\omega = \mu^2/2\eta$), and global softness ($\sigma = 1/\eta$). Global hardness indicates an atom's resistance to charge transfer, while softness refers to its ability to accept electrons [39].

Table 3. Electronic properties obtained through DFT B3LYP/6-311G

Molecule	HOMO	HOMO-1	LUMO	LUMO+1	E_g	χ	μ	η	s ($\times 10^{-1}$)	ω	σ ($\times 10^{-1}$)
DBSA	−1.57	−2.37	2.51	2.86	4.09	−0.47	0.47	2.04	2.45	0.054	4.8
SDS	−1.79	−2.33	2.74	3.21	4.53	−0.70	0.70	2.50	2.00	0,10	4,0
EG	−7.22	−7.25	1.65	3.05	8.88	2.78	−2.78	4.43	1.12	0.87	2.2
DEG	−6.93	−7.30	1.50	1.90	8.44	2.71	−2.71	4.21	1.18	0.87	2.4
AD	−7.37	−7.75	0.15	0.61	7.52	3.61	−3.61	3.76	1.33	1.73	2.6

* HOMO, HOMO-1, LUMO, LUMO+1 and E_g in (eV)

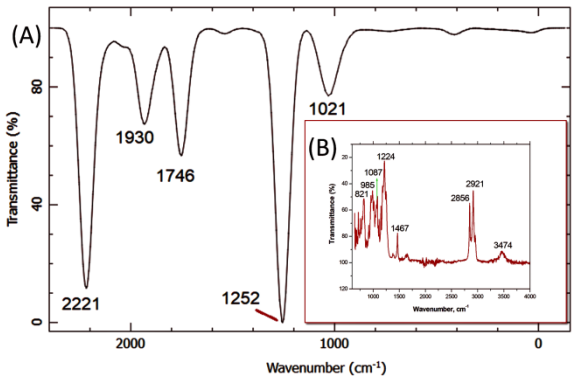

Fig. 11. Infrared spectra of the molecule of SDS (A) theoretical (B) experimental.

The theoretical study provides the anharmonic vibrational spectra of isolated forms of SDS, DBSA, EG, DEG, and AD. The wavenumbers obtained from both treatments are compared to experimental data.The IR theoretical and experimental spectra of the SDS molecule are presented in Figure 11. Pure SDS showed a sharp band at 985 cm^{-1} and a broad band at 821 cm^{-1}, which are attributable to S–O–C; –S=O stretch frequency appears at 1224 cm^{-1}. The bands at 2856 – 2921 cm^{-1} can be attributed to the C–H *str.* vibration. The difference between the spectra is due to the solid conformation for experimental data and the gaseous molecule for theoretical data. Comparatively, the experimental bands are 2221 cm^{-1} (C–H stretch), 1930 cm^{-1} ($-SO_2$), 1746 cm^{-1} (C=O stretch), 1252 (–S=O stretch) and 1021 cm^{-1} characteristic group frequency of SO_4^{2-}.

3. Material and Methods

3.1 Chemicals

Adipic Acid, AD (Sigma), acetylsalicylic acid (Merk), Citric acid (Merk), ethylene glycol, EG (Neon), diethylene glycol, DEG (Sigma), glycerol, GLY (ACS reagent), ionic liquid 1-Butyl-3-methylimidazolium chloride (Merck), polyethylene glycol, PEG (Sigma-Aldrich), tin chloride (Rottinger), zinc chloride (Dinâmica), sulfuric acid (Neon), hydrochloric acid (Vetec), tin (Merk), sodium dodecyl sulfate, SDS (Sigma-Aldrich), dodecyl benzene sulfonic acid, DBSA (Sigma-Aldrich), methanol (Merk), dimethylformamide, DMF (Vetec), chloroform (Hexis), THF (Vertec), were used without further purification and deionized water was used.

3.2 Instruments

Infrared spectroscopy analysis was performed with Spectrum 400 FT-MIR / FT-NIR - Perkin Elmer, in attenuated total reflectance (ATR) mode, 16 scans, with a resolution of 4 cm^{-1}. ^{1}H-NMR spectroscopy were measured in a Varian 400 MHz at 9.4 T, 5 mm BroadBand1H/X/D NMR probe with chloroform-d ($CDCl_3$) solution and 5% DMSO as a cosolvent, chemical shifts (δ)in ppm relation to tetramethylsilane (TMS). Thermal analyses were conducted with DSC Q200 (TA Instruments) controlled by software Universal V4.7; with approximately 5 mg of the sample at heating rates of 10 ºC·min^{-1} with 50 mL/min N_2 flow in the temperature range of -80 / 600 °C for DSC.

3.3 Surface tension and CMC measurements

Surface tensions were measured using a Lauda TD3 tensiometer equipped with a Pt-Ir Dü-nouy ring, with resolution of (±0.01 mN/m, ±0.1 mg). All measurements were performed using solutions at temperature range 25-65 ºC. For determining the CMC of surfactant solution, specific conductivity data were measured using a conductometer. The reproducibility of the conductivity measurements was within ±0.2 %.

3.4 Polymerization Procedure

The microemulsion polymerization reactions were adapted from the descriptions by Nakamura *et al.* (1979) [41], Tanaka *et al.* (2003) [4], Takasu *et al.* (2006) [5] and Jönsson *et al.* (2013) [42]: in an aqueous medium, in a 300 mL Schlenk-type reactor, 200 mL of deionized water and 0.5 g of surfactant (SDS or DBSA) were added, and the mixture was stirred. After complete dissolution of the surfactant, 3.0 g of adipic acid or acetylsalicylic acid and 5.0 mL of DEG, EG, glycerol, or other polyester-forming reagent (depending on the experiment performed) were added with gentle stirring. After a few minutes, one of the catalysts was added for each test performed (1.0 mL of HCl, 1.0 mL of H_2SO_4, or 3.0 g of $ZnCl_2$). The reactions were carried out at maximum temperatures of 40 °C, 60 °C, 75 °C, and 95 °C for 20 hours. After this time, the system was cooled to room temperature, and 100 mL of methanol were added to remove excess monomers. The solids formed were separated by filtration, washed and dried

in an oven at 40 °C for 6 hours.

3.5 Theoretical methods

All molecules structures were generated by hand using the Avogadro software; we then pre-optimized geometries at the semiempirical PM7 Hamiltonian with MOPAC2016 (Molecular Orbital PACkage) [43] and optimized with DFT B3LYP hybrid functional with a 6-31G(d,p) basis set [44]. The ORCA program [45] was used to perform the DFT calculations. The OPLS-AA force field [46] was used and parametrizations of all molecules have been done by using the automatic Web-based parameter generators LigParGen [47] and MKTOP [48]. Packmol software [49] was used to build the entire micelle-water assembly. The SDS micelle consisted of 60 surfactant molecules (the experimental value is 65 at the CMC) [50], and the DBSA micelle consisted of 90 surfactant molecules (the experimental value is approximately 93 at the CMC) [20]. All MD simulations were carried out with the GROMACS-2021.5 [51]. Each micelle-water system was inserted into a cubic box with an edge of 6.0 nm and 17500 water molecules were added, 0.2 nm distance tolerance.

4. Conclusions

Classical techniques for examining the characteristics of micellar systems employed in the production of polyesters generate outcomes in line with those reported in literature. Knowledge of the micelle shape, number of aggregates and interfacial phenomena are fundamental to comprehending the interactions between the polymer and surfactant throughout the reaction procedure. Moreover, supplementing the findings with MD and DFT assists in clarifying the properties of the reagents and surfactants utilized in the reaction process. Further studies should be conducted to improve the results found in this work.

Acknowledgments

The authors gratefully thanks to analysis by Nucleus of Competences in Petrochemical Chemistry (NCQP-UFES) for instrumentation.

Author Contributions

Vadilson Malaquias dos Santos: Conceptualization, writing – original draft, writing – review & editing, Methodology. Fabrício Uliana: Formal analysis, investigation. Rayanne Penha W. Lima: Formal analysis, investigation. Eloi Alves da Silva Filho: Supervision, Resources, Funding acquisition.

References and Notes

[1] Rabnawaz, M.; Wyman, I.; Auras, R.; Cheng, S. *Green Chem.* **2017**, *19*, 4737. [Crossref]

[2] Feghali, E.; Tauk, L.; Ortiz, P.; Vanbroekhoven, K.; Eevers, W. *Polym. Degrad. Stab.* **2020**, *179*, 109241. [Crossref]

[3] Diaz, C.; Mehrkhodavandi, P. *Polym. Chem.* **2021**, *12*, 783. [Crossref]

[4] Tanaka, H.; Kurihashi, T. *Polym. J.* **2003**, *35*, 359. [Crossref]

[5] Takasu, A.; Takemoto, A.; Hirabayashi, T. *Biomacromolecules* **2006**, *7*, 6. [Crossref]

[6] Benítez, J. J.; García-Segura, R.; Heredia, A. *Biochim. Biophys. Acta (BBA)* **2004**, *1674*, 1. [Crossref]

[7] Fan, Z.; Zhao, Y.; Preda, F.; Clacens, J.-M.; Shi, H.; Wang, L.; Feng, X.; De Campo, F. *Green Chem.* **2015**, *17*, 882. [Crossref]

[8] Lovell, P. A.; Schork, F. J. *Biomacromolecules* **2020**, *21*, 4396. [Crossref]

[9] Santos, M. S.; Tavares, F. W.; Biscaia Jr., E. C. Braz. *J. Chem. Eng.* **2016**, *33*, 515. [Crossref]

[10] Larsson, J.; Sanchez-Fernandez, A.; Leung, A. E.; Schweins, R.; Wu, B., Nylander, T.; Ulvenlund, S., Wahlgren, M. J. *Colloid Interface Sci.* **2021**, *581*, 895. [Crossref]

[11] Stubbs, S.; Yousaf, S.; Khan, I. *DARU J. Pharm Sci.* **2022**, 30, 407. [Crossref]

[12] Hendrikse, R. L.; Bayly, A. E.; Jimack, P. K. *J. Phys. Chem. B* **2022**, *126*, 8058. [Crossref]

[13] Goddard, E. D. *J. Colloid Interface Sci.* **2002**, *256*, 228. [Crossref]

[14] La Mesa, C. *J. Colloid Interface Sci.* **2005**, *286*, 148. [Crossref]

[15] Cabane, B.; Duplessix, R. *J. Phys.* **1987**, *48*, 651. [Crossref]

[16] Froehner, S. J.; Belarmino, A.; Zanette, D. *Colloids Surf. A* **1998**, *137*, 131. [Crossref]

[17] Haydukivska, K.; Blavatska, V.; Paturej, J. *Sci. Rep.* **2020**, *10*, 14127. [Crossref]

[18] Kasaai, M. R. *Carbohydrate Polymers* **2007**, 68, 477. [Crossref]

[19] Janczuk, B.; Zdziennicka, A.; Wójcik, W. *Colloids Surf. A* **2003**, *220*, 61. [Crossref]

[20] Almásy, L.; Artykulnyi, O. P.; Petrenko, V. I.; Ivankov, O. I.; Bulavin, L. A.; Yan, M.; Haramus, V. M. Molecules, **2022**, *27*, 2573. [Crossref]

[21] Gracie, K.; Turner, D.; Palepu, R. *Can. J. Chem.* **1996**, *74*, 1616. [Crossref]

[22] Shah, S. S.; Jamroz, N. U.; Sharif, Q. N. *Colloids Surf. A* **2001**, *178*, 199. [Crossref]

[23] Khan, H.; Seddon, J.; Law, R.; Brooks, N.; Robles, E.; Cabral, J.; Ces, O. *J. Colloid Interface Sci.* **2018**, *538*, 75. [Crossref]

[24] Artykulnyi, O. P.; Petrenko, V. I.; Bulavin, L. A.; Ivankov, O. I.; Avdeev, M. V. *J. Mol. Liq.* **2018**, *276*, 808. [Crossref]

[25] Mészáros, R.; Thompson, L.; Bos, M., Varga, I.; Gilányi, T. *Langmuir* **2003**, *19*, 609. [Crossref]

[26] Peacock, J. M.; Matijević, E. *J. Colloid Interface Sci.* **1980**, *77*, 548. [Crossref]

[27] Kim, B.-S.; Park, S. W.; Hammond, P. T. *ACS Nano* **2008**, *2*, 386. [Crossref]

[28] Tang, C.; McInnes, B. T. Molecules **2022**, *27*, 5611. [Crossref]

[29] Antunes, F. E.; Marques, E. F.; Miguel, M. G.; Lindman, B. *Adv. Colloid Interface Sci.* **2009**, *147*, 18. [Crossref]

[30] Choudhary, M.; Kamil, S. M. *ACS Omega* **2020**, *5*, 22891. [Crossref]

[31] Zhu, Y.; Free, M. L.; Woollam, R.; Durnie, W. *Prog. Mater. Sci.* **2017**, *90*, 159. [Crossref]

[32] Kékicheff, P. *J. Colloid Interface Sci.* **1989**, *131*, 133. [Crossref]

[33] Duplâtre, G.; Ferreira Marques, M. F.; da Graça Miguel, M. *J. Phys. Chem.* **1996**, *100*, 16608. [Crossref]

[34] Mieczkowski, R. *Eur. Polym. J.* **1991**, *27*, 377. [Crossref]

[35] Salaniwal, S.; Cui, S. T.; Cochran, H. D.; Cummings, P. T. *Langmuir* **2001**, *17*, 1773. [Crossref]

[36] Storm, S.; Jakobtorweihen, S.; Smirnova, I.; Panagiotopoulos, A. Z. *Langmuir* **2013**, *29*, 11582. [Crossref]

[37] Palazzesi, F.; Calvaresi, M.; Zerbetto, F. *Soft Matter* **2011**, *7*, 9148. [Crossref]

[38] Suzuki, S.; Green, P. G.; Bumgarner, R. E.; Dasgupta, S., Goddard; W. A., Blake; G. A. *Science* **1992**, *257*, 942. [Crossref]

[39] Koopmans, T. *Physica 1* **1934**, 104. [Crossref]

[40] Liu, Y.; Huang, K.; Zhou, Y.; Gou, D.; Shi, H. *J. Phys. Chem. B* **2021**, *125*, 8099. [Crossref]

[41] Nakamura, H.; Imanishi, S.; Sanui, K.; Ogata, N. *Polym. J. (Tokyo, Jpn.)* **1979**, II, *8*, 661. [Link]

[42] Jönsson, J. B.; Müllner, M.; Piculell, L.; Karlsson, O. J. *Macromolecules* **2013**, *46*, 9104. [Crossref]

[43] Stewart, J. J. *J. Comput.-Aided Mol. Des.* **1990**, *4*, 1. [Crossref]

[44] Becke, A. D. A. *J. Chem. Phys.* **1993**, *98*, 1372. [Crossref]

[45] Neese, F.; Wennmohs, F.; Becker, U.; Riplinger, C. *J. Chem. Phys*. **2020**, *152*, 224108. [Crossref]

[46] Jorgensen, W. L.; Tirado-Rives, J. *J. Am. Soc.* **1988**, *110*, 1657. [Crossref]

[47] Dodda, L. S.; Vaca, I. C.; Tirado-Rives, J.; Jorgensen, W. L. *Nucleic Acids Res*. **2017**, *45*, W1. [Crossref]

[48] Ribeiro, A. A. S. T.; Horta, B. A. C.; Alencastro, R. B. *J. Braz. Chem. Soc.* **2008**, *19*, 7. [Crossref]

[49] Martínez, L.; Andrade, R.; Birgin, E. G.; Martínez, J. M. *J. Comput. Chem.* **2019**, *30*, 2157. [Crossref]

[50] Petrenko, V. I.; Avdeev, M. V.; Garamus, V. M.; Bulavin, L. A.; Aksenov, V. L.; Rosta, L. *Colloids Surf., A* **2010**, *369*, 160. [Crossref]

[51] Van Der Spoel, D.; Lindahl, E.; Hess, B.; Groenhof, G.; Mark, A. E.; Berendsen, H. J. C. *J. Comput. Chem.* **2005**, *26*, 1701. [Crossref]

How to cite this article

Dos Santos, V. M.; Uliana, F.; Lima, R. P. W.; da Silva Filho, E. A *Orbital: Electron. J. Chem.* **2024**, *16*, 182. DOI: http://dx.doi.org/10.17807/orbital.v16i3.20153